TUDelft

Delft University of Technology

Experimental and numerical study on lateral resistance of frictional sleeper with arrowhead groove

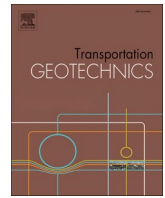Jing, Guoqing; Jia, Wenli; Wang, Xinyu; Markine, Valeri; Nålsund, Roar; Guo, Yunlong

Important note
To cite this publication, please use the final published version (if applicable).
Please check the document version above.

Experimental and numerical study on lateral resistance of frictional sleeper with arrowhead groove

Guoqing Jing [a], Wenli Jia [b], Xinyu Wang [a], Valeri Markine [b], Roar Nålsund [c], Yunlong Guo [b],*

[a] *School of Civil Engineering, Beijing Jiaotong University, Beijing 100044, China*
[b] *Faculty of Civil Engineering and Geosciences, Delft University of Technology, Delft 2628CN, Netherlands*
[c] *Bane NOR (Norwegian National Rail Administration), Trondheim 7020, Norway*

ARTICLE INFO

ABSTRACT

To enhance the stability of continuous welded rail (CWR) tracks, frictional sleepers have been developed. The frictional sleepers are new types of sleepers with grooves on the bottom, and different bottom grooves improve lateral resistances at different magnitudes. In this study, single sleeper push test (SSPT) and its model with discrete element method (DEM) were carried out to confirm how much arrowhead groove frictional (AGF) sleeper increases the lateral resistance of ballasted track. The SSPTs were performed to confirm the lateral resistance results, and also to validate and calibrate the DEM models. With the validated models, the groove factors influencing the lateral resistances were studied, including groove sizes (depth, width), arrowhead groove direction and groove numbers. The reason of lateral resistance improvement was studied at mesoscopic level, including the ballast-sleeper contact numbers and contact force chains. Results show that applying the AGF sleeper is able to improve lateral resistance by 7–24%, and it can provide enough lateral resistance after reducing ballast shoulder width from 500 mm to 300 mm. The AGF sleeper can improve the sleeper-ballast interaction by increasing sleeper-ballast contact number. The study is helpful for frictional sleeper design, further improving track stability.

Introduction

Ballasted track is a common railway structure that is widely-used worldwide with many advantages, e.g. low construction cost, easy maintenance and high transportation capability [1,2]. For increasing train speed and axle load, the majority of the jointed tracks have been changed to the CWR tracks in the last decades all over the world [3–7]. The CWR track has become the typical modern track structure with plenty of advantages [8]. Specifically, comparing with the jointed tracks, the CWR tracks are able to reduce the maintenance cost, increase the lifespans of the tracks and vehicles, increase the ride comfort and reduce traction energy costs and noises [9–11].

Even though the CWR tracks have plenty of advantages, track bulking as one significant CWR track stability issue still needs to be solved. More importantly, the track bulking can considerably increase the possibility of derailments. The track buckling normally happens at the lateral direction, while it sometimes also appears at the vertical direction. This phenomenon is mainly induced due to the rail temperature change and train accelerating or braking, meanwhile the ballast bed is

not able to provide enough lateral resistances to the sleepers. Particularly, it becomes severer when there exists the rail eccentricity because of the track irregularities at some special areas (bridges, bends and tunnels).

To improve the track stability (improving lateral resistance), many studies have been performed at the practical means, and the means were classified into three aspects [12]. Firstly, innovative materials were applied in the ballast bed. The innovative materials consist of the ballast glue [13], geogrid [14–16], geocell [17–19], crumb rubber chips [20,21], steel slag [22–24], rubber-protected ballast [25,26] and under ballast pads [27–31]. It is confirmed that using these materials can improve the track stability. Specifically, the lateral resistance of ballast bed increases at 42% with the geocell [14,32]. Applying the ballast glue improves the lateral resistance at 31% [33], while the lateral resistance is improved at 27% when replacing the ballast to steel slag [23].

Moreover, the track stability has been improved by strengthening the ballast-sleeper interactions. To be more specific, using wider ballast shoulder width and higher shoulder height has been proved effective to improve ballast lateral resistance, until the resistance reaches a

---

* Corresponding author.
  E-mail address: yunlong.guo@tudelft.nl (Y. Guo).

maximum value [4]. Applying the sleeper anchor can improve the lateral resistance by 50% [10].

Most importantly, new sleeper designs have been applied to improve the lateral resistance of ballast bed (Fig. 1), including Y-shaped sleeper, ladder sleeper, sleeper with wings [6,34], steel sleeper, nailed sleeper [5] and frictional sleeper [35]. New sleeper designs were developed at the aspects of using different sleeper materials or shapes. It was proved that the new designs are able to provide larger lateral resistance

[5,6,34–37]. To be more specific, the winged-shape sleeper can improve the lateral resistance by 50%, frictional sleeper by 70% and nailed sleeper by 200%.

Among the technical means, the frictional sleeper has attracted more and more focus with many advantages. The frictional sleeper is made by shaping different grooves at normal sleeper bottom [35]. The advantages are: (1) lateral resistance improvement, (2) lower costs, the frictional sleeper is easier to produce with some certain moulds; (3) easier

a. Y-shape sleeper (reproduced from [37])

b. Ladder sleeper (reproduced from [36])
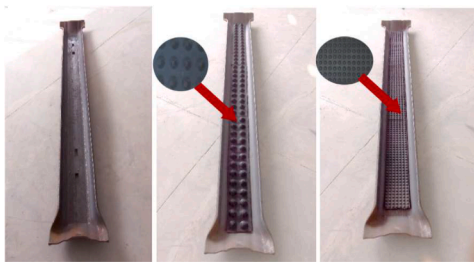
c. Steel sleeper (reproduced from [37])

d. Frictional sleeper (reproduced from [38])

e. Winged-shape sleeper (reproduced from [34])

f. Nailed sleeper

g. Sleeper anchor (figure reproduced from [39])

Fig. 1. New sleeper designs from earlier studies. (See above-mentioned references for further information.)

installation, the frictional sleeper can be installed as normal track construction process; and (4) easier maintenance, the frictional sleeper does not interrupt or change maintenance process.
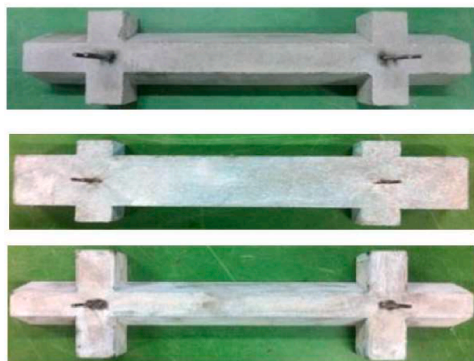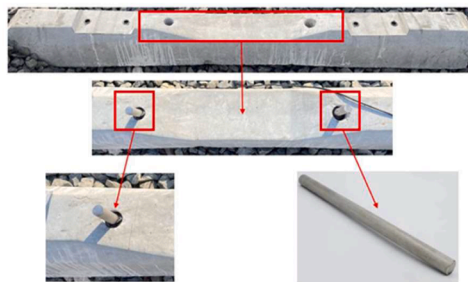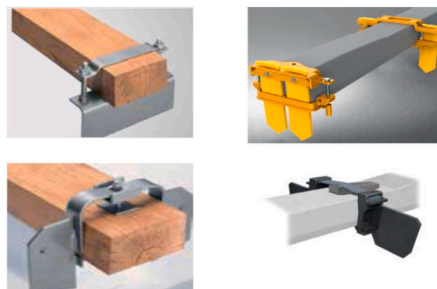
Because of the advantages, the frictional sleeper becomes an attractive solution to improve track stability (lateral resistance), and many studies have been performed including laboratory tests and field tests. For example, in [35,40,41], the lateral resistance of frictional sleeper (grooves, Fig. 1d) was studied with laboratory tests, experimental tests and finite element method (FEM) modelling. From the results, it has been confirmed that using this kind of frictional sleeper (grooves) can increase the lateral resistances at 63–70% (FEM results), 67% (field track panel results) and 64% (experimental results), respectively. Moreover, in [38] different bottom shapes were studied with experimental tests and discrete element modelling, proving that the frictional sleepers (three types, Fig. 1d) increase the lateral resistance by improving ballast-sleeper interaction.

In order to optimise the groove shape of frictional sleepers and find the optimal one, the experimental tests and discrete element modelling were performed in this study. The lateral resistance of arrowhead groove frictional (AGF) sleeper was studied, and how to design the arrowhead groove was confirmed. It needs to note that the arrowhead grooves have been applied in the Norwegian railway line, however, to date no studies were performed for this type of sleeper. The AGF sleeper is worth to study, because the arrowhead groove has more contact areas between sleeper bottom and ballast, which can lead to higher lateral resistance of ballast bed. Note that the sleeper bottom can provide at least 35% of the lateral resistance through three parts of sleeper-ballast contacts (Fig. 2), i.e. base ballast (bottom force), shoulder ballast (end force) and crib ballast (side force).

The single sleeper push tests (SSPTs) were performed to obtain the lateral resistance results, and the results were used to validate and calibrate the DEM models of the SSPTs. Through the models, the factors of groove shapes influencing the lateral resistances were studied, including groove sizes (depth, width), arrowhead groove direction and groove numbers. In addition, the reason of lateral resistance improvement was studied at mesoscopic level, including the contact number between sleeper and ballast and contact force chain.

The study is helpful for sleeper design, and further for the track stability improvement. More importantly, the frictional sleeper (arrowhead groove) can be applied in some special railway structures, e. g. ballast beds at curves or on bridges (or tunnels). Specifically, on the bridges the ballast bed profile is reduced due to the bridge capacity, while at the curves only one side of the lateral resistance (outer rail side) should be improved. By designing different arrowhead grooves can promisingly solve these two issues.

Methodology

Single sleeper push test

Single sleeper push test (SSPT) is a test to obtain displacement-force relationship. The displacement is obtained by measuring sleeper displacement, and the force is obtained by measuring the force of pushing the sleeper. The SSPT is a widely-used method to test track stability, especially for the track buckling prevention [3]. The SSPTs were performed to calibrate the DEM models and also to
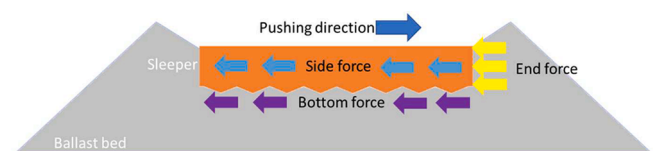

Fig. 2. Lateral resistance contribution from different parts.

Materials

Ballast. The ballast material used for the bed construction is basalt, which is provided by Tangshan Quarry. The material properties including durability, hardness and mineralogy, etc. were tested, and the results are given in Table 1. The test results meet the British standard requirement for ballast material, which proves that the basalt can be used to build ballast bed.

Moreover, the particle size distribution (PSD) is shown in Fig. 3, and it meets the requirement of the British standard [42]. The SSPT was performed on a ballast bed that is built based on the ballast track design code for high speed railway [43]. The ballast thickness under the sleeper is 350 mm, and the slope is 1:1.75, which is required in the Chinese design code for high speed railway [43]. In addition, the shoulder ballast width is 500 mm with shoulder height at 0 mm.

Sleeper. As shown in Fig. 4a, three types of frictional sleepers were made on the base of Chinese mono-block sleeper with different grooves attached at the sleeper bottom. The three different grooves were inward arrowhead groove, outward arrowhead groove and single direction arrowhead groove (Fig. 4). The groove size is presented in the figure, and the groove thickness is 15 mm. The different grooves were designed for different track structures. The single direction arrowhead groove sleeper can be applied for the curve to improve the one-side lateral resistance (outer rail side), and the other two can be used in the normal track or ballast bed on the bridges (or tunnels). A normal sleeper was used for comparison, which is commonly-used in Chinese railway, mono-block sleeper. The mono-block sleeper size is shown in Fig. 4b.

Test setup

As show in Table 2, the conditions of single sleeper push tests are given. Note that the single direction AGF sleeper needs to be pushed at two opposite directions (Condition A2 and C4), considering that possibly their lateral resistances are of big differences. Each test condition was performed three times, and the average values were taken as the final results.

The test conditions were decided to answer four questions. 1. How much the AGF sleeper can improve the lateral resistance. 2. How much the lateral resistance of single direction AGF sleeper is different from that of the inward or outward AGF sleepers. 3. Whether the AGF sleeper can provide enough lateral resistance when applied at a ballast bed with its profiled reduced. 4. How much resistance the AGF sleeper bottom can provide, and what percentage of resistance the sleeper bottom can take.

For the fourth question, due to the AGF sleeper mainly increases the interaction between ballast and sleeper bottom, and the contribution of sleeper bottom to the lateral resistance is around 35% [4]. Therefore, it is necessary to know how much using the arrowhead groove increases lateral resistance of ballast bed, and particularly the resistance value and its corresponding percentage of the sleeper bottom can also be used for DEM model calibration.

Test procedure

The single sleeper push test setup is shown in Fig. 5. The frictional sleepers installed on the compacted ballast bed. Then, ballast particles

Table 1
Ballast material properties (reproduced from [38]).

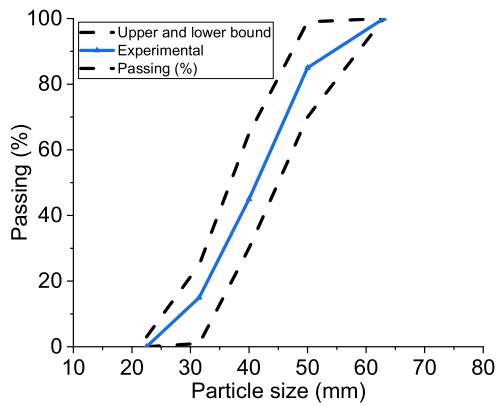| Property	Standard	Result	Maximum specification value
Micro-Deval loss (%)	BS EN 1097-1	5.20	7.00
Flakiness index (%)	BS EN 93-3	2.20	35.00
Elongation index (%)	BS EN 93-3	0.90	4.00
Fine particle content (%)	BS EN 933-1	0.30	0.60
Fines content (%)	BS EN 93-3	0.20	0.50

Fig. 3. Particle size distribution of ballast bed.

were filled as ballast shoulder and crib with a compactor compacting them. At one side of the AGS sleeper (Fig. 5), a hydraulic jack was used to push the sleeper, and a pressure sensor was placed between the jack and a steel rod. The steel rod was motionless, which can be used to provide enough support to push the sleeper. The pressure sensor as connected to the data acquisition system (IMC). The dial indicator was placed at the other side of the AGF sleeper to measure the corresponding sleeper displacement. Finally, the displacement-force curves were obtained. Note that each AGF sleeper was loaded by two sleepers for 24 h and then the two sleepers were removed before performing the SSPTs. Though this process, the contacts between sleeper and ballast were improved, which was more similar to the field track condition.

After setting the facilities, the SSPTs were started by pushing the sleeper by step loadings. Every loading step was finished when the pushing force was stable (30 s' interval). The SSPT was finished, when the pushing force reached and kept the maximum value as long as the sleeper displacement increased. The test facilities and their parameters are given in Table 3, including hydraulic jack, data acquisition system, dial indicator and pressure sensor.

Single sleeper push test model

The single sleeper push test model in this study was built with the discrete element method (DEM) software, particle flow code (PFC), because it can be applied to obtain important ballast mechanical properties, such as, displacements, contact force chain and acceleration [44,45]. In addition, it has a deeper insight of ballast mechanical behaviour and degradation mechanisms under various loading conditions [17,46–48].

The software contains two kinds of basic elements: balls and walls [49]: the railway ballast were modelled as a number of spheres to resemble real particles [50,51], as shown in Fig. 6a, and all the particle

models applied in this study are shown in Fig. 6b. The sleepers were as the combination of several walls (Fig. 6c). The ballast bed is made of the modelled ballast particles and sleeper, as shown in Fig. 6d.

Ballast particle creation

Fig. 6a shows the flow chart of ballast particle creation based on 3-D images. The first step is to scan several typical ballast particles (with different shapes and sizes) to obtain their 3-D images. One 3-D image is made of lots of small triangle meshes [53,54]. The 3-D image is reconstructed by the surface points (obtained by laser scanning) with connecting each three neighbouring points forming a facet. Based on the 3-D images, the second step is to create the uncrushable particle, the Clump, which is built by several spheres [55].

In the first step, in order to simulate more accurately, ballast particles with different shapes, including cubic, the flaky or elongated particles are scanned. The shape classification is based on the definition in [53]. 20 ballast particles in total with different shapes are scanned as a library. Each ballast particle consists of around 20 spheres.

In the second step, when building the Clumps, two significant parameters are applied to decide the shape accuracy, i.e. ρ and φ, as shown in Fig. 7 [55]. The ρ and φ can confirm the sphere number, and more spheres make more accurate Clump shape as real particle (Fig. 7).

The value of the two parameters, ρ and φ, should be determined before simulating the tests of WRC. On one hand, the value of φ and ρ determines the particle accuracy, which effects the contacts and interlocking between the Clumps, mechanical behaviour and load response [47,50]. On the other hand, the ρ determines the diameter of small Pebbles, which generally are at the particle corner and edge.

A particle shape library was built with the introduced particle creation method, and all the ballast particles were generated based on the library (Fig. 6b).

Table 2
Single sleeper push test conditions.

Test condition	Groove type	Shoulder width (mm)	Slope	Crib ballast
A1	None (mono-block sleeper)	500	1:1.75	Yes
A2	Single direction arrowhead groove (two pushing directions)	500	1:1.75	Yes
A3	Inward arrowhead groove	500	1:1.75	Yes
A4	Outward arrowhead groove	500	1:1.75	Yes
B1	Single direction arrowhead groove	300	1:1.75	Yes
C1	None (mono-block sleeper)	0	0	No
C2	Inward arrowhead groove	0	0	No
C3	Outward arrowhead groove	0	0	No
C4	Single direction arrowhead groove (two pushing directions)	0	0	No
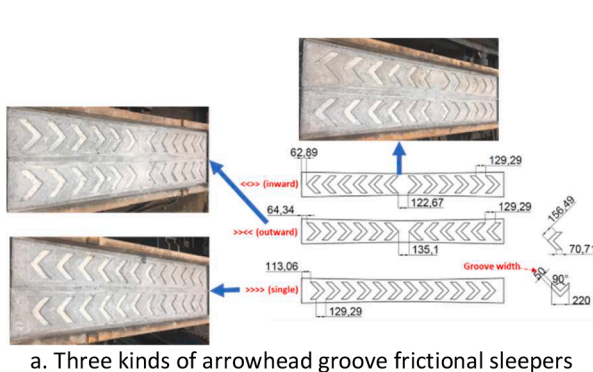
a. Three kinds of arrowhead groove frictional sleepers
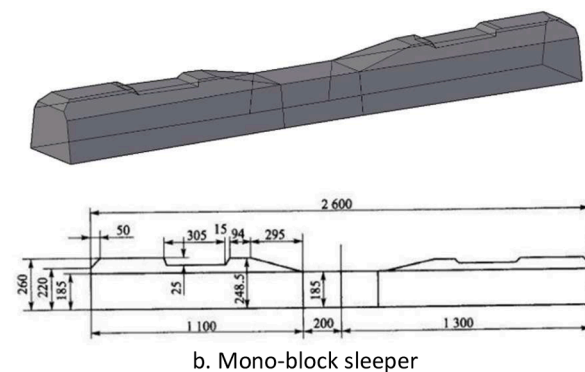
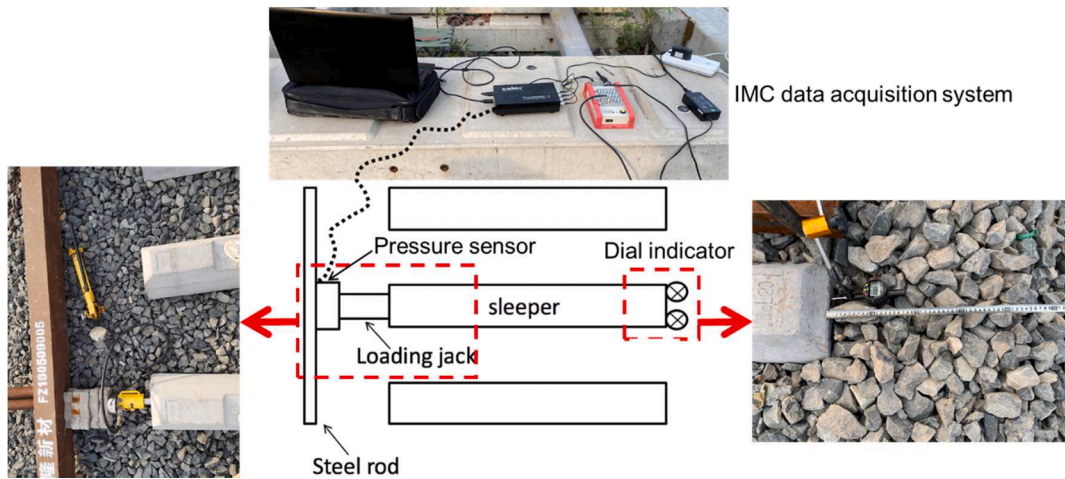b. Mono-block sleeper

Fig. 4. Sleepers in single sleeper push tests.

Fig. 5. Single sleeper push test setup.

Table 3
Test facilities and facility parameters.

Facility name	Parameters
Hydraulic jack	Maximum loading: 10 ton; Actuator stroke: 10 cm
Data acquisition system	Name: IMC; Product model: INV3018A
Dial indicator	Precision 0.001 mm; measuring range 0–30 mm,
Pressure sensor	Measuring range: 0–10 ton

Sleeper creation

Several kinds of sleepers with different arrowhead grooves were drawn in the software, AutoCAD. After that, the 3D sleeper drawings were exported to the "stl" format. With the drawings that contains the sleeper configurations, the Walls were applied to build the sleeper models (Fig. 6c). The modelled sleeper types are given in Table 4. In the table, the groove width is one description for the groove shape, as shown in Fig. 4.

Ballast bed creation

Note that most the contents in this section are reproduced from the reference [38]. Because the same model construction method was used in this paper. In this section, the SSPT model creation is introduced. The first step was building a profile geometry to contain particles using the Wall command, as shown in Fig. 8a. The second step was generating basic elements, spheres, in the profile geometry according to the experimental PSD until the porosity reached 0.30. The last step was replacing the spheres using the Clumps with an algorithm.

Particularly, the modelled ballast particles (from 3D images) were used to make the ballast bed, and the ballast particles were generated with a self-developed method for faster model creation by fast stress (between particles) equilibrium (will be introduced later). Before the generation of ballast particles, the sleeper (Wall elements) was generated and fixed at the certain position until the ballast bed stabilised. The detail steps of the model creation are as follows.

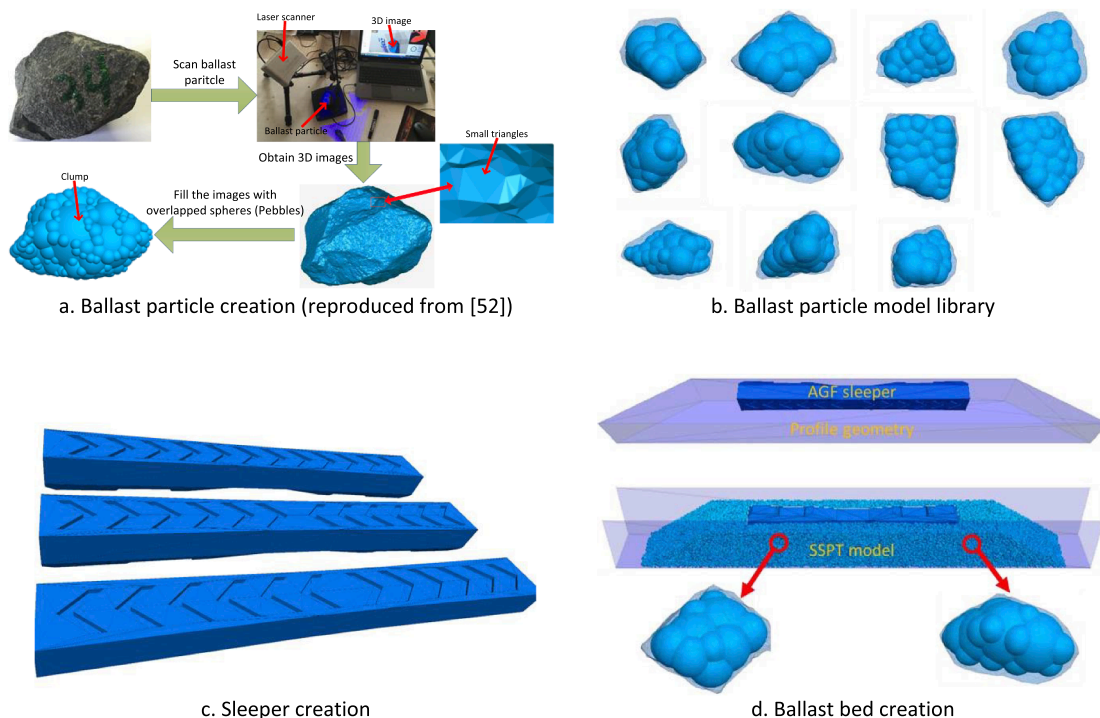Firstly, a profile geometry is created for containing the ballast

a. Ballast particle creation (reproduced from [52])

b. Ballast particle model library

c. Sleeper creation

d. Ballast bed creation

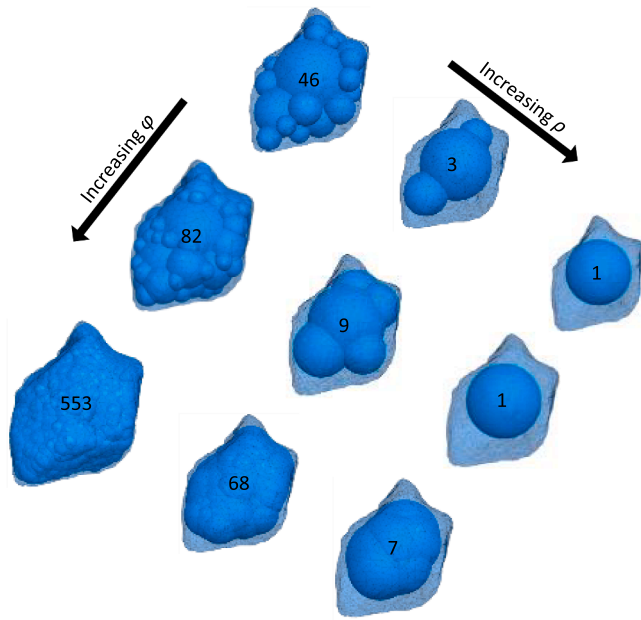**Fig. 6.** Discrete element method model construction procedure.

Fig. 7. Ballast particle (clump) creation demonstration (reproduced from [52]).

Table 4
Modelled arrowhead groove frictional sleeper types.

Sleeper number	Arrowhead groove direction	Groove width (mm)	Groove number
Mono-block sleeper	–	–	–
AGF sleeper 1	≫≪ (outward)	50	12
AGF sleeper 2	≪≫ (inward)	50	12
AGF sleeper 3	≫≫≫ (single)	50	12
AGF sleeper 4	≪≫ (inward)	40	16
AGF sleeper 5	≪≫ (inward)	60	10

particles with the Wall command, as shown in Fig. 8a. The two side walls were made into slopes, which is the same slope grade (1:1.75) as the ballast shoulder. The ballast shoulder width is 500 mm, and the ballast thickness is 350 mm. The ballast bed slope is 1: 1.75 and the length of the ballast bed is 600 mm.

Afterwards, the spheres are generated in the profile geometry with the same PSD as the experimental tests. The sphere generation keeps on until the required porosity (0.30) is reached. During the generation process, the sleeper is fixed at the certain position. Due to the sphere is randomly generated in the geometry, there are many overlaps between spheres. Therefore, the model should be stabilised with high damping forces until the ratio of unbalanced contact forces to average contact

forces is below 0.01. This stage is named the initial equilibrium state.

Finally, the spheres are replaced with Clumps with the self-develop algorithm, which can make that the Clump has the correct volume, density and position. More importantly, the algorithm guarantees a little change at the contact forces between particles. Specifically, as shown in Eq. (1), a scaling factor (β) is confirmed based on the contact force. The scaling factor is a factor used to expand the clump size. The algorithm is shown in Eq. (1). In the equation, the scaling factor (β) was firstly decided according to the contact forces between Clumps. The scaling factor is defined as how much to expand sizes of each clumps, and it is decided by the sphere radius (R_i^a), ballast bed volume (V_b), target ballast bed stress (σ_{in}), present average ballast bed stress (σ_m) and normal stiffness between spheres (k_i^n) [38].

(a) $\beta = -1 \cdot \lambda \cdot V_b \cdot \Delta\sigma \cdot k_{sum}^n$

(b) $\Delta\sigma = \sigma_{in} - \sigma_m$ 　　　　(1)

(c) $k_{sum}^n = \sum_i \left(k_i^n \cdot \left(R_i^a + R_i^b \right) \cdot R_i \right)$

After the model was built, a preloading (two times heavier sleeper) was applied in the model to simulate the preloading in the experimental tests.

SSPT model parameters

The linear contact model (LCM) was applied in the DEM models. The contact model was applied between clumps or between clumps and walls. In the contact model, several parameters need to define, including normal stiffness, shear stiffness, friction and damping. Moreover, other SSPT model parameters should be defined as well, i.e., particle density. The SSPT model parameters were calibrated based on the test results, which are the same in [38] as shown in Table 5.

At the contacts, two types of components are used i.e., a spring and a dashpot to transmit and dissipate kinetic energy. The spring is set through the normal and shear stiffnesses, and the dashpot is set through damping. The normal and shear stiffnesses are set by comparing simulation results to the test results. The friction is also decided by the test results, because complex particle (clump) does not need to set high friction value, which is usually very high when applying the spheres as ballast particles. The damping is set according to the earlier studies [52]. In most of the studies, the damping value is set as 0.7. The density is set according the ballast that is used in the SSPTs. The particle density is

Table 5
Parameters for the SSPT models (reproduced from [38]).

Parameters	Clump	Wall
Normal stiffness, k_n (N/m)	5e9	1e9
Shear stiffness, k_s (N/m)	2e9	1e9
Friction	0.55	0.55
Density (kg/m³)	2700	–

a. Profile geometry　　b. Sphere filling in the geometry
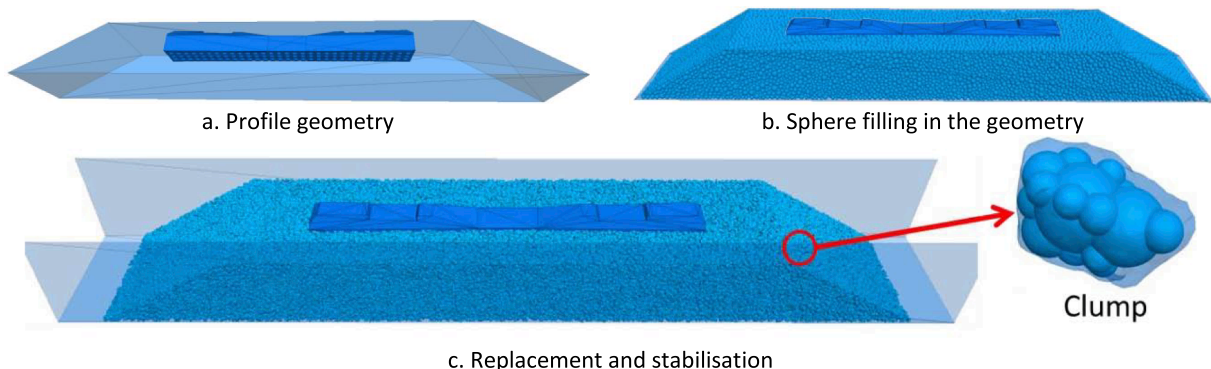
c. Replacement and stabilisation

Fig. 8. SSPT model creation procedure (figure reproduced from [38]).

defined the same as the ballast density in the SSPT tests.

Results and discussions

Test results, discussions and model validation

Test results and discussions

Fig. 9 presents the SSPT results, including (1) lateral resistance of all AGF and mono-block sleepers; (2) lateral resistances of pushing single direction AGF sleeper at two directions (opposite to or same with the arrowhead direction); (3) lateral resistance of single direction AGF sleeper after reducing shoulder ballast width from 500 mm to 300 mm; (4) contribution of the sleeper bottom to the total lateral resistance of AGF and mono-block sleeper. Note that in the figure the single direction, inward direction and outward direction are the three types of AGF sleepers (Fig. 4). The opposite pushing direction means the direction of pushing the AGF sleeper is opposite to the arrowhead direction, while the same pushing direction means the direction of pushing the AGF sleeper is the same as the arrowhead direction.

From Fig. 9a, it can be observed that all the resistances of the AGF sleepers are higher than mono-block sleeper at 7–24%. The resistances of inward direction AGF sleeper and outward direction AGF sleeper are approximate, which means either of them can be applied to replace common sleepers.

Fig. 9b summarises the lateral resistances of single direction AGF sleeper at two pushing directions, and the resistances are compared with that of the mono-block sleeper. The figure presents that the lateral

resistances are of considerable difference at two pushing directions at approximately 20%. When the pushing direction was the same as the arrowhead direction (single direction AGF sleeper), the lateral resistance is 7% higher. With the same sleeper, the lateral resistance is 24% higher with the pushing direction opposite to the arrowhead direction. This means that the single direction AGF sleeper can be applied to ballast beds at curves, because it can improve lateral resistance of one side and the other side keeps normal and sufficient lateral resistance value.

Fig. 9c summarises the lateral resistances of single direction AGF sleeper with 300 mm or 500 mm ballast shoulder width and mono-block sleeper with 500 mm ballast shoulder width. From the figure, it can be seen that after reducing ballast shoulder width from 500 to 300 mm the lateral resistance reduces at 16%, but the resistance of the AGF sleeper (300 mm width) is still approximate to the mono-block sleeper (normal sleeper). This means the AGF sleeper can be applied for the ballast beds with its profile reduced at some special structures, e.g. bridges and tunnels.

Fig. 9d summarises contributions of different AGF sleeper bottoms to the total lateral resistance (sleeper side, end and bottom; Fig. 2). From the figure, it can be observed that the contributions of the AGF sleeper bottom are from 43.9% to 47.7%, which are higher than that of the mono-block sleeper (37.3%). This means the sleeper bottom can provide almost half of the lateral resistance, furthermore, the AGF sleeper can provide enough lateral resistance when the shoulder ballast width or height are reduced.

a. Lateral resistances of AGF and mono-block sleepers

b. Lateral resistances of different directions of pushing single direction AGF sleeper

c. Lateral resistance after reducing shoulder ballast width
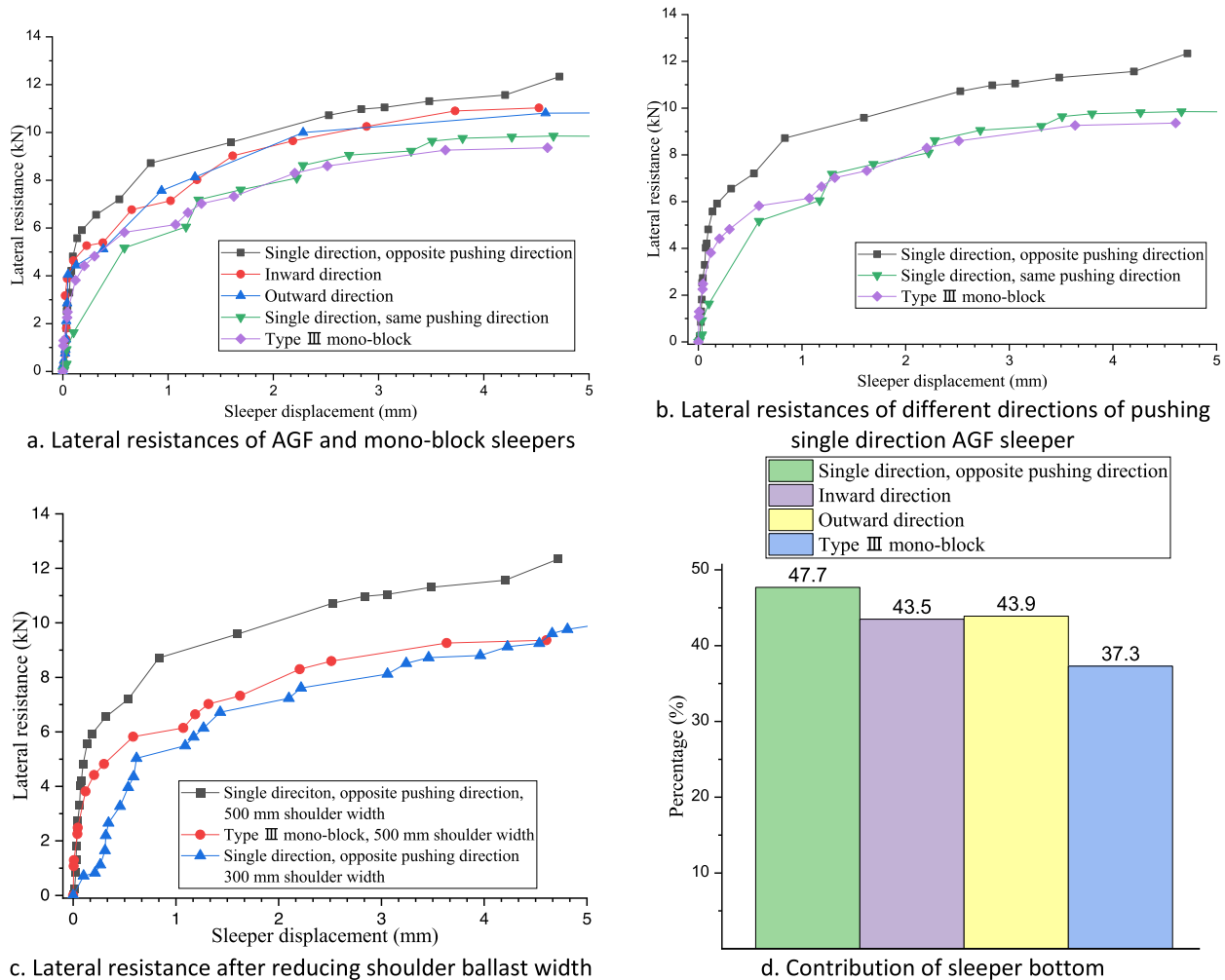

d. Contribution of sleeper bottom

Fig. 9. Test results of lateral resistance and contribution of bottom ballast.

Model validation

Fig. 10 summarised the comparison of numerical simulation results and experimental results. From the figure, it can be concluded that the simulation results are approximate to the experimental results, which means the model can be used for further analysis on other types of AGF sleeper design. The other types of AGF design are to change the bottom groove shapes, as described in Table 4.

The applied model parameters are the same as ones in [38]. The normal and shear stiffnesses are used to calculate the contact forces, which are according to the Young's modulus and Poisson ratio as described in [38]. The friction is applied at the shear direction of particle relative motions (or particle–wall), and the density is the same as the ballast density used in the experimental tests.

From Fig. 10, some mismatches of experimental and numerical results can be seen. The main reason for the mismatches are explained as follows. Firstly, the ballast bed is made of ballast particles, which means the ballast bed has the discrete nature with high possibility of deformation. The deformation usually comes with local contact force chain failure, which causes the result mismatches. For example, the local compaction degree (at sleeper-ballast shoulder) may be different from the overall ballast bed compaction. In addition, the sudden change of local contact force also leads to result mismatch. For example, some ballast particles are forced to rotation, and some ballast particles have less contacts with the neighbouring ballast particles. The two conditions lead to more rotations of ballast particles, further failure of local ballast contact force chain. However, we have controlled the mismatch as less as possible by using the same particle size distribution of ballast particles and same porosity (compaction). Even though there are still some small mismatches, they are within the tolerance.

Numerical results and discussions

Using the validated model with calibrated parameters, more types of AGF sleepers were performed with SSPT simulations, as shown in Table 4. In the table, AGF sleeper 1–3 and mono-block sleeper were used for model validation and parameter calibration, and the AGF sleeper 4/5 were used for comparing the lateral resistance improvements. Furthermore, the models were used to study the reason of lateral resistance improvement at mesoscopic level, including the contact number between sleeper and ballast and contact force chain.
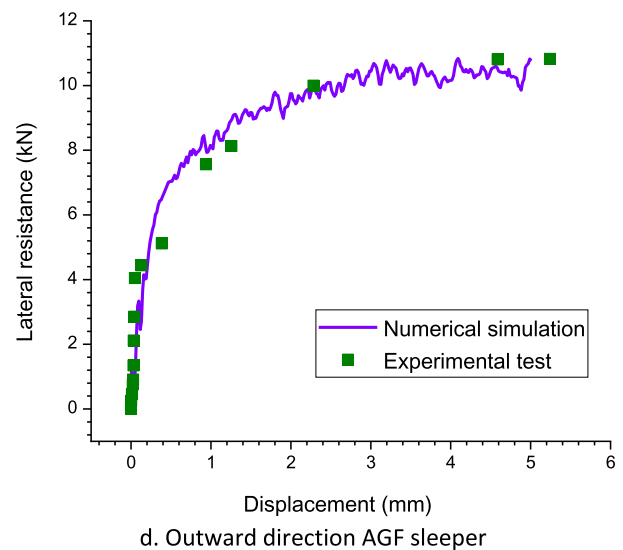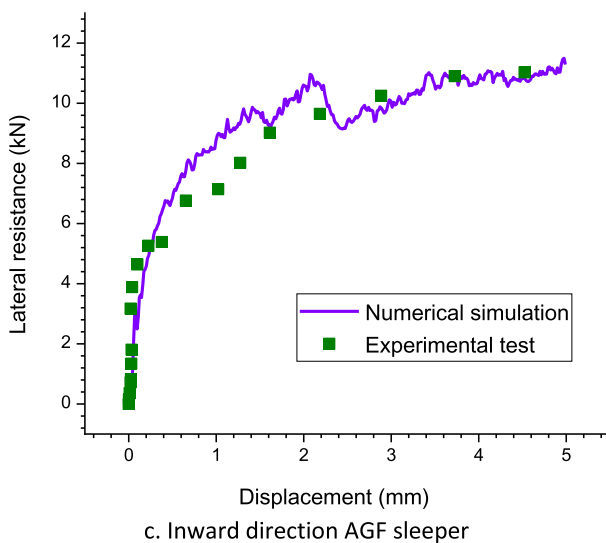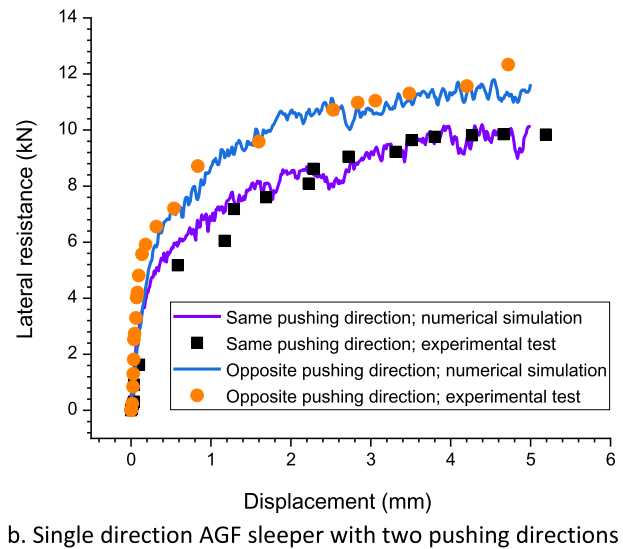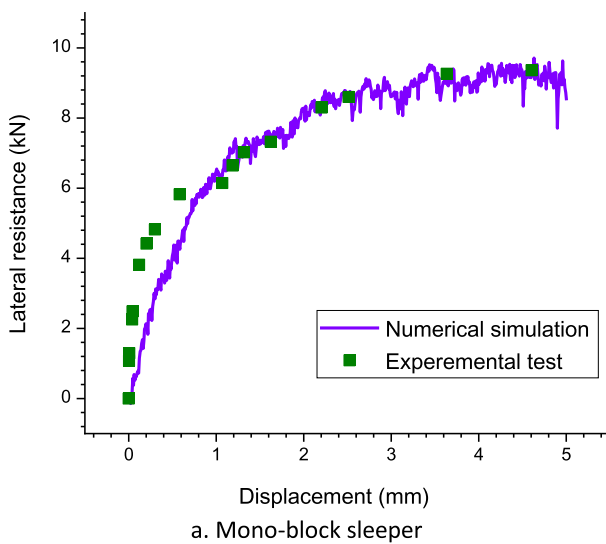

Fig. 10. Comparison of numerical simulation results and experimental test results.

Lateral resistances

The lateral resistances of the AGF sleepers 2, 4 and 5 (Table 4) were summarised in Fig. 11. The figure presents all the AGF sleepers provide higher lateral resistances than the lateral resistance of mono-block sleeper. AGF sleeper 5 provides the highest lateral resistances, which means that wider groove can provide higher lateral resistance. In addition, even though the AGF sleeper 4 has the most grooves (16) that is higher than AGF 2 or 5 (12 or 12), the lateral resistance of AGF sleeper 4 is the lowest. This means groove number has less influences on lateral resistance than the groove width. Possibly, this is due to ballast particles can have better interaction when the groove width is wider, which means the ballast particles can be inserted in the groove. Deeper exploration on this phenomenon is presented in the following sections from the sleeper-ballast contact perspective.

It can be seen that the AGF sleeper-2 (red line) drops suddenly at 2 mm sleeper displacement. The reason is explained as follows. When the sleeper displacement is less than 2 mm, the sleeper and the ballast particles usually have the static friction. When the sleeper moves over 2 mm, some frictions become static friction or rolling friction. Due to the friction change, the former interlock of sleeper and ballast was changed, then lateral resistance will drop suddenly when the interlock is broken.

Contact number

Fig. 12 summarised the contact number of sleeper-ballast. From the figure, it can be seen that the lowest contact number is the single arrowhead direction AGF sleeper with same pushing direction (AGF sleeper 3), which is much lower than mono-block sleeper (92). The ballast-sleeper contact number of normal sleeper is approximate to the number in [38], which means the model is reliable. This means it needs to be careful when applying the single arrowhead AGF sleeper, especially pay attention to the installing direction at curves. The highest contact number is the AGF sleeper 4, which has 16 arrowhead grooves. This proves more arrowhead grooves more sleeper-ballast contacts. By summarising the lateral resistances and contact number, it can be concluded that more contacts in most cases lead to higher lateral resistances. In addition, more contacts have the ability to provide higher resistance, because more ballast particles join in providing resistances.

Contact force chain

Fig. 13 presents the contact forces at the end of SSPTs. From the figure, it can be seen that mono-block sleeper (Fig. 13a) and the AGF sleeper 3 with same pushing direction (Fig. 13d) have less intensive
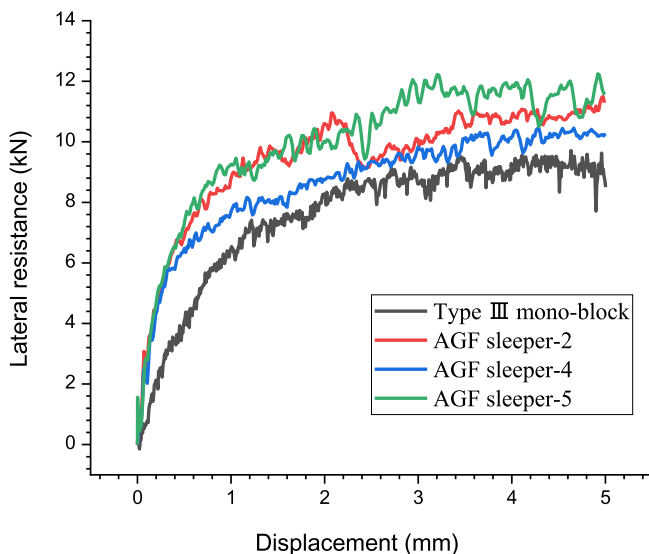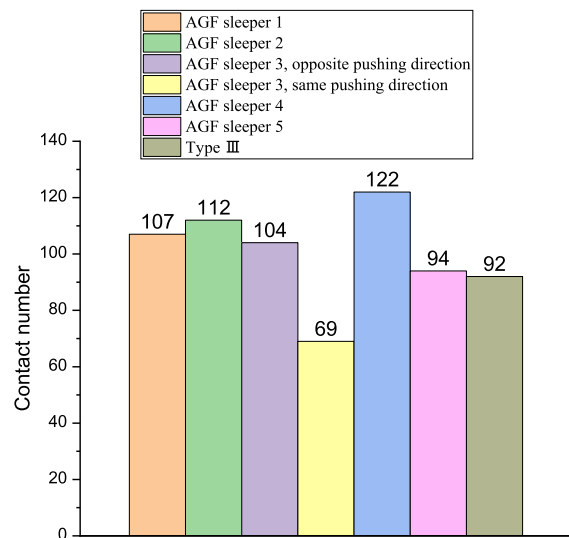

Fig. 12. Contact number between sleeper bottom and ballast particles.

contact forces than the other five (Fig. 13b/c/e/f/g). This reflects that higher lateral resistance is due to that more ballast particles contribute to higher contact forces, making stronger contact force chain. More importantly, the AGF sleeper can improve not only the contacts between sleeper bottom and ballast particles, but also the contacts between ballast particles.

By comparing the contact force chain with the earlier study [38], the same conclusion that more ballast particles join in providing lateral resistance was obtained. Furthermore, the groove difference has considerable influences on the contact force distribution. The sleeper bottom groove is sunken in this study, while the bottom groove is bulgy in [38]. The AGF sleeper can be built as prefabricated concrete, while the frictional sleeper in [38] was made by attaching materials to the normal sleeper. The AGF sleeper is easy to produce, and it can have longer service life, because sunken grooves can be protected.

Conclusions and perspectives

Conclusions

This paper focused on one type of frictional sleeper, arrowhead groove frictional sleeper (AGF sleeper) to study (1) how much the AGF sleeper can improve lateral resistance; (2) proper arrowhead groove design (groove number, shape) and (3) reason investigation of lateral resistance improvement from mesoscopic level. To study these, the laboratory test (SSPT) and SSPT models were applied. After analysing the results, the following conclusion can be given:

1. The AGF sleeper can improve lateral resistance at 7–24%, more importantly, the AGF with ballast shoulder width at 300 mm can still provide approximate lateral resistance to normal sleeper with ballast shoulder width at 500 mm. This means the AGF sleeper can be used for some special structures (e.g. bridges, tunnels).
2. When using the single direction AGF sleeper for curves, the arrowhead direction should point to the inner rail.
3. The arrowhead groove width is an important factor influencing the lateral resistance improvement. Groove width at 60 mm can provide higher lateral resistance than 40 mm groove width.
4. The main reason of lateral resistance improvement (using AGF sleeper) is that the sleeper-ballast interaction is improved, which leads to that more ballast particles join in providing resistances.
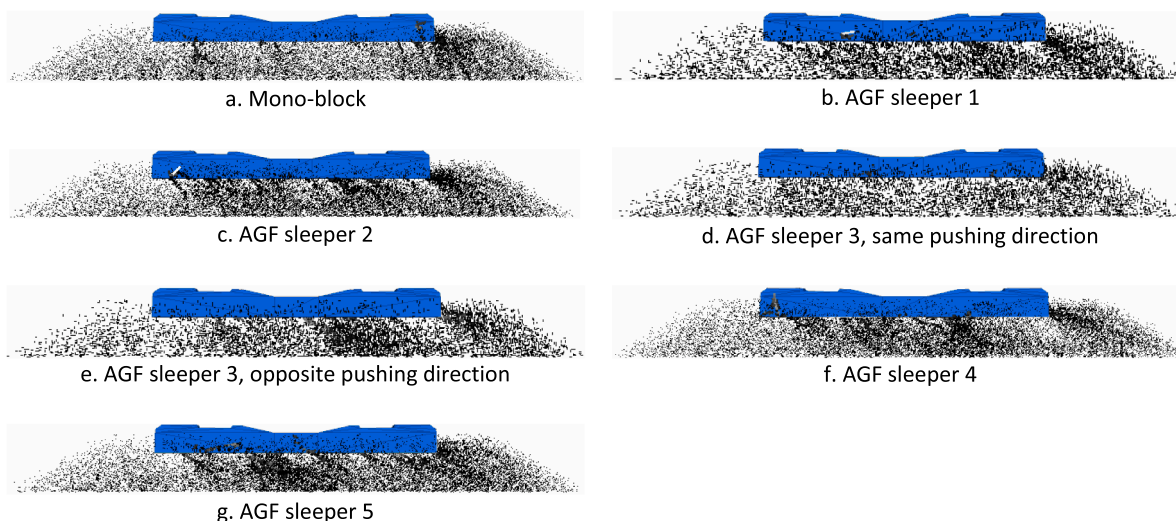

Fig. 11. Lateral resistances of numerical simulations with SSPTs on AGF sleepers.

a. Mono-block   b. AGF sleeper 1

c. AGF sleeper 2   d. AGF sleeper 3, same pushing direction

e. AGF sleeper 3, opposite pushing direction   f. AGF sleeper 4

g. AGF sleeper 5

Fig. 13. Contact force of ballast particles.

Perspectives

Due to the resistances were measured under unloaded conditions, further studies will be performed on the real track loading conditions. Deeper analysis will be performed on the shear band and direction of contact force chain.

CRediT authorship contribution statement

Guoqing Jing: Funding acquisition, Resources, Writing – review & editing, Supervision. **Wenli Jia:** Formal analysis, Investigation, Visualization, Software. **Xinyu Wang:** Formal analysis. **Valeri Markine:** Writing – review & editing, Resources, Supervision. **Roar Nålsund:** Writing – review & editing. **Yunlong Guo:** Formal analysis, Investigation, Data curation, Methodology, Validation, Writing – original draft, Writing – review & editing.

Declaration of Competing Interest

The authors declare that they have no known competing financial interests or personal relationships that could have appeared to influence the work reported in this paper.

Acknowledgements

References

[1] Indraratna B, Ngo T. Ballast railroad design: smart-UOW approach. CRC Press; 2018.
[2] Li D, Hyslip J, Sussmann T, Chrismer S. Railway geotechnics. CRC Press; 2002.
[3] Kish A, Samavedam G. Track buckling prevention: theory, safety concepts, and applications. US: John A. Volpe National Transportation Systems Center; 2013.
[4] Powrie W, Le Pen LM. Contribution of base, crib, and shoulder ballast to the lateral sliding resistance of railway track: a geotechnical perspective. Proc Instit Mech Engineers, Part F: J Rail Rapid Transit 2011;225(2):113–28.
[5] Esmaeili M, Khodaverdian A, Neyestanaki HK, Nazari S. Investigating the effect of nailed sleepers on increasing the lateral resistance of ballasted track. Comput Geotech 2016;71:1–11.
[6] Koike Y, Nakamura T, Hayano K, Momoya Y. Numerical method for evaluating the lateral resistance of sleepers in ballasted tracks. Soils Found 2014;54(3):502–14.
[7] Chen M, Sun Y, Zhai W. High efficient dynamic analysis of vehicle–track–subgrade vertical interaction based on Green function method. Veh Syst Dyn 2019;58(7):1076–100.
[8] D C. European Rail Research Institute, Improved knowledge of forces in CWR track (including switches). Report 2, review of existing experimental work in behaviour of CWR track. Utrecht: European Rail Research Institute; 1995.
[9] Lim NH, Han SY, Han TH, Kang YJ. Parametric Study on Stability of Continuous Welded Rail Track - Ballast Resistance and Track Irregularity-. Int J Steel Struct 2008;8(3):171–81.
[10] Zarembski A. Survey of techniques and approaches for increasing the lateral resistance of wood Tie track. Newark: Department of Civil and Environmental Engineering, University of Delaware; 2016.
[11] Pucillo GP, Penta F, Catena M, Lisi S. On the lateral stability of the sleeper-ballast system. Procedia Struct Inte 2018;12:553–60.
[12] Liu J, Wang P, Liu G, Xiao J, Liu H, Gao T. Influence of a tamping operation on the vibrational characteristics and resistance-evolution law of a ballast bed. Constr Build Mater 2020;239:117879.
[13] Kennedy J, Woodward P, Medero G, Banimahd M. Reducing railway track settlement using three-dimensional polyurethane polymer reinforcement of the ballast. Constr Build Mater 2013;44:615–25.
[14] Esmaeili M, Zakeri JA, Babaei M. Laboratory and field investigation of the effect of geogrid-reinforced ballast on railway track lateral resistance. Geotext Geomembr 2017;45(2):23–33.
[15] Chen C, Indraratna B, McDowell G, Rujikiatkamjorn C. Discrete element modelling of lateral displacement of a granular assembly under cyclic loading. Comput Geotech 2015;69:474–84.
[16] Qian Y, Mishra D, Tutumluer E, Kazmee HA. Characterization of geogrid reinforced ballast behavior at different levels of degradation through triaxial shear strength test and discrete element modeling. Geotext Geomembr 2015;43(5):393–402.
[17] Ngo NT, Indraratna B, Rujikiatkamjorn C, Mahdi Biabani M. Experimental and discrete element modeling of geocell-stabilized subballast subjected to cyclic loading. J Geotech Geoenviron Eng 2016;142(4):04015100.
[18] Kaewunruen S, Remennikov A, Aikawa A. Effectiveness of soft baseplates and fastenings to mitigate track dynamic settlement at transition zone at railway bridge approaches. Proceedings of the third international conference on railway technology: research, development and maintenance. Civil-Comp Press; 2016.
[19] Liu Y, Deng A, Jaksa M. Three-dimensional modeling of geocell-reinforced straight and curved ballast embankments. Comput Geotech 2018;102:53–65.
[20] Fathali M, Nejad FM, Esmaeili M. Influence of tire-derived aggregates on the properties of railway ballast material. J Mater Civ Eng 2017;29(1):04016177.
[21] Sol-Sánchez M, Thom NH, Moreno-Navarro F, Rubio-Gámez MC, Airey GD. A study into the use of crumb rubber in railway ballast. Constr Build Mater 2015;75:19–24.
[22] Esmaeili M, Yousefian K, Nouri R. Vertical load distribution in ballasted railway tracks with steel slag and limestone ballasts. Int J Pavement Eng 2017;20(9):1065–72.
[23] Esmaeili M, Nouri R, Yousefian K. Experimental comparison of the lateral resistance of tracks with steel slag ballast and limestone ballast materials. Proc Instit Mech Engineers, Part F: J Rail Rapid Transit 2016;231(2):175–84.
[24] Qi Y, Indraratna B, Heitor A, Vinod JS. Effect of rubber crumbs on the cyclic behavior of steel furnace slag and coal wash mixtures. J Geotech Geoenviron Eng 2018;144(2).
[25] Sol-Sánchez M, Moreno-Navarro F, Rubio-Gámez M, Manzo N, Fontseré V. Full-scale study of Neoballast section for its application in railway tracks: optimization of track design. Mater Struct 2018;51(2):43.
[26] Fontserè V, Pita AL, Manzo N, Ausilio A. NEOBALLAST: new high-performance and long-lasting ballast for sustainable railway infrastructures. Transp Res Procedia 2016;14:1847–54.
[27] Li H, McDowell GR. Discrete element modelling of under sleeper pads using a box test. Granular Matter 2018;20(2).

[28] Navaratnarajah SK, Indraratna B, Ngo NT. Influence of under sleeper pads on ballast behavior under cyclic loading: experimental and numerical studies. J Geotech Geoenviron Eng 2018;144(9):04018068.

[29] Le Pen L, Watson G, Hudson A, Powrie W. Behaviour of under sleeper pads at switches and crossings – Field measurements. Proc Inst Mech Eng F J Rail Rapid Transit 2018;232(4):1049–63.

[30] Kaewunruen S, Aikawa A, Remennikov AM. Vibration attenuation at rail joints through under sleeper pads. Procedia Eng 2017;189:193–8.

[31] Lima AdO, Dersch MS, Qian Y, Tutumluer E, Edwards JR. Laboratory fatigue performance of under-ballast mats under varying loads and support conditions. Proc Instit Mech Engineers, Part F: J Rail Rapid Transit 2019;233(6):606–13.

[32] Indraratna B, Hussaini SKK, Vinod J. The lateral displacement response of geogrid-reinforced ballast under cyclic loading. Geotext Geomembr 2013;39:20–9.

[33] Jing G, Zhang X, Jia W. Lateral resistance of polyurethane-reinforced ballast with the application of new bonding schemes: Laboratory tests and discrete element simulations. Constr Build Mater 2019;221:627–36.

[34] Ichikawa T, Hayano K, Nakamura T, Momoya Y. Lateral resistance of ballasted tracks for various shapes of sleepers based on limit equilibrium methods. Jpn Geotech Soc Special Publ 2016;2(46):1632–5.

[35] Ali Zakeri J, Esmaeili M, Kasraei A, Bakhtiary A. A numerical investigation on the lateral resistance of frictional sleepers in ballasted railway tracks. Proc Instit Mech Engineers, Part F: J Rail Rapid Transit 2014;230(2):440–9.

[36] Jing G, Aela P, Fu H. The contribution of ballast layer components to the lateral resistance of ladder sleeper track. Constr Build Mater 2019;202:796–805.

[37] Jing G, Fu H, Aela P. Lateral displacement of different types of steel sleepers on ballasted track. Constr Build Mater 2018;186:1268–75.

[38] Guo Y, Fu H, Qian Y, Markine V, Jing G. Effect of sleeper bottom texture on lateral resistance with discrete element modelling. Constr Build Mater 2020;250.

[39] Jing GQ, Ji YM, Aela P. Experimental and numerical analysis of anchor-reinforced sleepers lateral resistance on ballasted track. Constr Build Mater 2020;264.

[40] Zakeri JA, Mirfattahi B. Field investigation on the lateral resistance of railway tracks with frictional sleepers. In: IOP conference series: materials science and engineering. IOP Publishing; 2020. p. 012125.

[41] Zakeri J-A, Mirfattahi B, Fakhari M. Lateral resistance of railway track with frictional sleepers. Proc Instit Civil Engineers – Transp 2012;165(2):151–5.

[42] British Standards Institution, Aggregates for railway ballast. London: British Standards Institution; 2013.

[43] N.R.A.o.t.P.s.R.o. China, Code for design of high speed railway. TB 1062-2014; 2014.

[44] Xiao J, Zhang D, Wei K, Luo Z. Shakedown behaviors of railway ballast under cyclic loading. Constr Build Mater 2017;155:1206–14.

[45] Zhang X, Zhao C, Zhai W. Dynamic behavior analysis of high-speed railway ballast under moving vehicle loads using discrete element method. Int J Geomech 2016;17(7):04016157.

[46] Indraratna B, Salim W, Rujikiatkamjorn C. Advanced rail geotechnology: Ballasted track. London: CRC Press; 2011.

[47] Lim WL, McDowell GR. Discrete element modelling of railway ballast. Granular Matter 2005;7(1):19–29.

[48] Qian J, Gu J, Gu X, Huang M, Mu L. DEM analysis of railtrack ballast degradation under monotonic and cyclic loading. Procedia Eng 2016;143:1285–92.

[49] C. Itasca, PFC (particle flow code in 2 and 3 dimensions), version 5.0 [User's manual], Minneapolis; 2014.

[50] Lu M, McDowell GR. The importance of modelling ballast particle shape in the discrete element method. Granular Matter 2006;9(1–2):69–80.

[51] McDowell GR, Li H. Discrete element modelling of scaled railway ballast under triaxial conditions. Granular Matter 2016;18(3).

[52] Guo Y, Zhao C, Markine V, Jing G, Zhai W. Calibration for discrete element modelling of railway ballast: A review. Transp Geotech 2020;23:100341.

[53] Anochie-Boateng JK, Komba JJ, Mvelase GM. Three-dimensional laser scanning technique to quantify aggregate and ballast shape properties. Constr Build Mater 2013;43:389–98.

[54] Sun Y, Indraratna B, Nimbalkar S. Three-dimensional characterisation of particle size and shape for ballast. Geotech Lett 2014;4:197–202.

[55] Taghavi R. Automatic clump generation based on mid-surface. In: Proceedings, 2nd international FLAC/DEM symposium, Melbourne; 2011. p. 791–7.